# Carrier-Phase Estimation Techniques for MIMO Optical Wireless Communication Systems

Kouki Seitaibashi and Shiro Ryu
*School of Advanced Mathematical Sciences, Meiji University*
4-21-1, Nakano, Nakano-ku, Tokyo 164-8525, Japan
cs223014@meiji.ac.jp

***Abstract*—We have compared three techniques for carrier-phase estimation in MIMO optical wireless communication systems. We have clarified that the symbol-by-symbol phase estimation method is the best among them.**

***Keywords— Optical wireless communications, MIMO, ZF, DCO-OFDM, phase estimation, phase correction***

## I. INTRODUCTION

The development of Internet technologies, such as smartphones and personal computers, has caused congestion in mobile networks and Wi-Fi. Optical wireless communication technology is being studied to solve line congestion [1]. Optical wireless communication, which uses different frequency bands from radio waves, is expected to increase transmission capacity. However, the modulation bandwidth of commercially available light-emitting diode (LED) is about 20 MHz, which is insufficient to provide large capacity [2]. Multi-input multi-output (MIMO) technology, which uses multiple transmitters and receivers, is attracting much attention in optical wireless communication systems [3-5]. In MIMO technology, the zero-forcing (ZF) method [3] is used to estimate the transmitted signal of each transmitter. In the ZF method, we have to estimate the phase of the received signal, which should be compensated in the signal recovery process. This paper describes methods to estimate the carrier phase in MIMO optical wireless communication systems. We use the preamble and postamble to estimate the carrier phase in the transmitted signal. We use three carrier-phase estimation methods, i.e., 1) ZF with the preamble, 2) ZF with the preamble and postamble, and 3) improved ZF by symbol-by-symbol phase estimation. After the experiments using the above three methods in single-carrier MIMO and direct current biased optical orthogonal frequency-division multiplexing (DCO-OFDM) MIMO systems [4,5], we have concluded that the improved ZF by symbol-by-symbol phase estimation is the best among the three techniques.

## II. MIMO TECHNOLOGY

### A. Single carrier MIMO

Fig. 1 shows the MIMO system. The propagation model of the MIMO system is expressed as

$$y = Hx + n. \tag{1}$$

Component representation of (1) is shown as follows,

$$\begin{pmatrix} y_1(t) \\ y_2(t) \\ \vdots \\ y_{Nr}(t) \end{pmatrix} = \begin{pmatrix} h_{11} & h_{12} & \cdots & h_{1Nt} \\ h_{21} & h_{22} & \cdots & h_{2Nt} \\ \vdots & \vdots & \ddots & \vdots \\ h_{Nr1} & h_{Nr2} & \cdots & h_{NrNt} \end{pmatrix} \begin{pmatrix} x_1(t) \\ x_2(t) \\ \vdots \\ x_{Nt}(t) \end{pmatrix} + \begin{pmatrix} n_1(t) \\ n_2(t) \\ \vdots \\ n_{Nr}(t) \end{pmatrix}, \tag{2}$$

where $x_j(t)$ is the transmitted signal of the $j$-th optical transmitter, $N_t$ is the number of transmitters, $y_i(t)$ is the received signal at the $i$-th optical receiver, $N_r$ is the number of receivers, $h_{ij}$ is the propagation constant between the $j$-th optical transmitter and the $i$-th optical receiver, and $n_i(t)$ is the noise of the $i$-th optical receiver.

Fig. 2 shows the modulation process of the single-carrier MIMO system in this paper. First, the pseudo-random binary sequence (PRBS) is generated. The PRBS for each transmitter has different initial values so we can distinguish the recovered data for TX1-4. Serial to parallel (S/P) conversion is performed for the PRBS signals, and 64QAM modulation was applied. The preamble and postamble are added to the data to estimate the carrier phase in the demodulation process [6]. Fig.3 shows the frame structure of the data. Four QPSK complex signals, i.e., 0.7+0.7$j$, -0.7+0.7$j$, -0.7-0.7$j$, and 0.7-0.7$j$, were used for the preamble and postamble. In measuring the propagation matrix, only one transmitter transmits the data to avoid interference from the other.

Fig.4 shows the demodulation process of single-carrier MIMO. First, complex signals were obtained by performing synchronous detection on the received signal. The propagation matrix was then estimated, and signal separation was performed. After the signal separation, each estimated symbol is parallel-to-serial (P/S) converted, and the data are recovered.

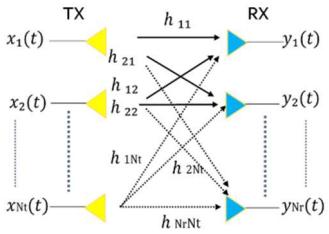


Fig.1. MIMO system.

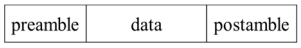


Fig.3. Frame structure of data.

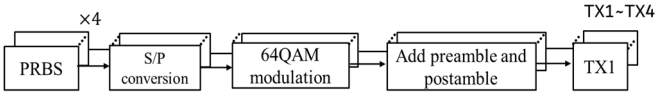


Fig.2. Modulation process of single-carrier MIMO.

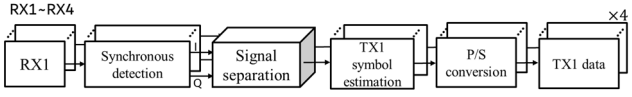


Fig.4. Demodulation process of single-carrier MIMO.

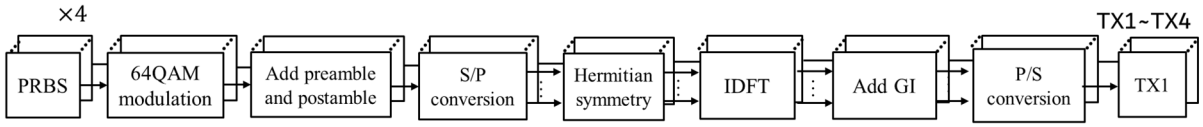


Fig.5. Modulation process of DCO-OFDM MIMO.

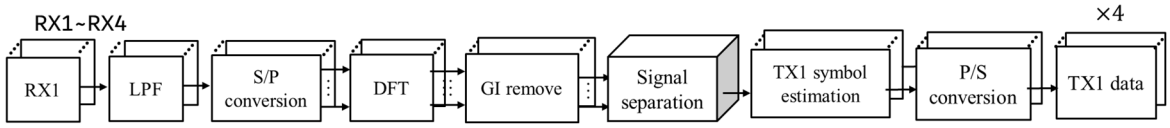


Fig.6. Demodulation process of DCO-OFDM MIMO.

### *B. DCO-OFDM MIMO*

Fig.5. shows the modulation process for DCO-OFDM MIMO [4,5,7]. Two sets of preamble and postamble are added to each carrier of the OFDM signal to estimate the propagation matrix. Then, the S/P conversion is performed to give Hermite symmetry to the frequency-domain signal, and the inverse discrete Fourier transform (IDFT) is applied to make the OFDM signal a real signal. Then, the guard interval (GI) is added, and the P/S conversion is performed to generate the transmit signal for each transmitter.

Fig.6 shows the demodulation process of the DCO-OFDM MIMO. First, the signal received at each receiver is introduced into the lowpass filter (LPF). Then, discrete Fourier transform (DFT) is applied to the S/P converted data. After removing the GI, the propagation matrix is estimated. Next, the signal separation was performed using the ZF method. After signal separation, each estimated symbol is subjected to P/S conversion. Then we can recover the data.

### *C. Channel Estimation Methods*

When channel estimation is performed, only $x_j$ is transmitted. The transmitted signal is a predetermined pilot signal with a preamble and postamble with a length of $L$ symbols. We find the propagation constant $h_{ij}$ between transmitter $j$ and receiver $i$ using the least squares method.

$$\sum_{t=1}^{L} x_j(t)^2 \neq 0 \tag{3}$$

$$f(h)=\sum_{t=1}^{L} (y_i(t) - h_{ij}x_j(t))^2 \tag{4}$$

$$\frac{df(h)}{dh}=2\sum_{t=1}^{L} x_j(y_i(t) - h_{ij}x_j(t))=0 \tag{5}$$

$$\widehat{h_{ij}}=\frac{\sum_{t=1}^{L} y_i(t)\,x_j(t)}{\sum_{t=1}^{L} x_j(t)^2}=\frac{Y_i X_j^T}{X_j X_j^T},\ \begin{pmatrix} X_j=[x_j(1)\ x_j(2)\ldots x_L(L)] \\ Y_i=[y_i(1)\ y_i(2)\ldots y_i(L)] \end{pmatrix} \tag{6}$$

where $f(h)$ is an evaluation function, and $\widehat{h_{ij}}$ is the estimated propagation constant. As seen from (6), the propagation constant can be obtained by calculating the expected value.

The following three methods are used to estimate the received carrier phase,

*1) ZF with preamble*
*2) ZF with preamble and postamble*
*3) Improved ZF by symbol-by-symbol phase estimation*

We describe each method in the following.

*1) ZF with preamble*

Fig.7 shows the signal processing method using the ZF method with an only preamble. Suppose that the preamble at transmitter 1 is $X_{pre1}$, the preamble received by receiver 1 is $Y_{pre1}$, $X_{pre1}$ and $Y_{pre1}$ can be expressed as

$$X_{pre1}=[0.7+0.7j, -0.7+0.7j, -0.7-0.7j, 0.7-0.7j] \tag{7}$$

$$Y_{pre1}=[y_{11}\ y_{12}\ y_{13}\ y_{14}]. \tag{8}$$

Fig.8(a) shows an example of received preambles ($Y_{pre1}$) in the single-carrier MIMO experiment. The carrier frequency was 10MHz. The propagation constant $h_{11}$ between transmitter 1 and receiver 1 is derived from (6) as

$$h_{11}=\frac{Y_{pre1}X_{pre1}^T}{X_{\mathrm{pre1}}X_{\mathrm{pre1}}^T}. \tag{9}$$

This calculation is performed for all transmitter-receiver combinations to obtain the propagation matrix $H_p$ in the following ($H_p$ is the propagation matrix obtained by the preamble),

$$H_p=\begin{bmatrix} h_{11} & h_{12} & h_{13} & h_{14} \\ h_{21} & h_{22} & h_{23} & h_{24} \\ h_{31} & h_{32} & h_{33} & h_{34} \\ h_{41} & h_{42} & h_{34} & h_{44} \end{bmatrix}. \tag{10}$$

Then, the ZF method is applied using the general inverse $W_p$ of $H_p$, $H_p^H$, and we can obtain the recovered signal [4].

$$W_p=(H_p^H H_p)^{-1} H_p^H \tag{11}$$

$$x_{ZFp}=W_p\, y. \tag{12}$$

*2) ZF with preamble and postamble*

Fig.7 shows the signal processing method using the ZF method with preamble and postamble. The propagation constant between transmitter 1 and receiver 1 is estimated using the preamble and postamble. If we denote the preamble and postamble of transmitter 1 as $X_{pre1}$ and $X_{post1}$, and the preamble and postamble of receiver 1 as $Y_{pre1}$ and $Y_{post1}$, respectively, they can be expressed as

$$X_{pre1}=[0.7+0.7j, -0.7+0.7j, -0.7-0.7j, 0.7-0.7j] \tag{13a}$$

$$X_{post1}=[0.7+0.7j, -0.7+0.7j, -0.7-0.7j, 0.7-0.7j] \tag{13b}$$

$$Y_{pre1}=[y_{11}\ y_{12}\ y_{13}\ y_{14}] \tag{13c}$$

$$Y_{post1}=[y_{15}\ y_{16}\ y_{17}\ y_{18}]. \tag{13d}$$

Fig.8(b) shows the received preamble and postamble ($Y_{pre1}$ and $Y_{post1}$) in the experiment. In the carrier phase estimation, the transmitted and received preamble and postamble are combined to generate $X_1$ and $Y_1$ as follows,

$$X_1=[X_{pre1}\ \ X_{post1}] \quad (1\times 8) \tag{14}$$

$$Y_1=[Y_{pre1}\ \ Y_{post1}] \quad (1\times 8). \tag{15}$$

The propagation constant $h_{11}$ between transmitter 1 and receiver 1 is derived as

$$h_{11}=\frac{Y_1 X_1^T}{X_1 X_1^T}. \tag{16}$$

Such calculation is performed for all the transmitter and receiver combinations to obtain the propagation matrix $H_s$ ($H_s$ is the propagation matrix obtained by a preamble and postamble)

$$H_s=\begin{bmatrix} h_{11} & h_{12} & h_{13} & h_{14} \\ h_{21} & h_{22} & h_{23} & h_{24} \\ h_{31} & h_{32} & h_{33} & h_{34} \\ h_{41} & h_{42} & h_{34} & h_{44} \end{bmatrix}. \tag{17}$$

Then, the ZF method is applied using the general inverse $W_s$ of $H_s$, $H_s^H$, and the received signal $y$.

$$W_s=(H_s^H H_s)^{-1} H_s^H \tag{18}$$

$$x_{ZFs}=W_s y. \tag{19}$$

*3) Improved ZF by symbol-by-symbol phase estimation*

This method applies phase compensation for each data considering the phase delay depending on the position of the data. The method is shown in Fig.9. The ZF method is applied using the general inverse $W_s$, and the received signal $y$. Fig.10(a) shows TX1 estimated by ZF using preamble and postamble, and its magnified view is shown in Fig.10(b), which confirms the phase delay due to data location. This phase delay is corrected by multiplying the phase correction vector generated from the preamble and postamble received at each receiver.

First, the receiver with the highest signal power for each transmitter is estimated, as shown in Fig.10(c). For example, some receivers in the experiment do not have a sufficient SNR for TX1 due to the transmitter-receiver configuration. If phase correction is performed using the preamble and postamble of a receiver that does not have a sufficient SNR, it will be affected by noise.

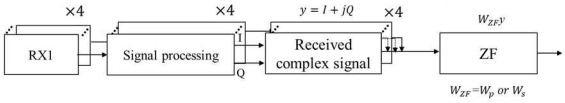


Fig.7. ZF using preamble and postamble

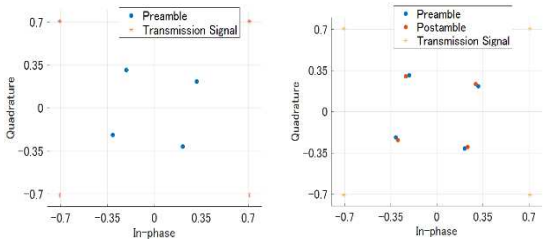


(a) preamble (b)preamble and postamble

Fig.8. Received constellation of a pilot signal.

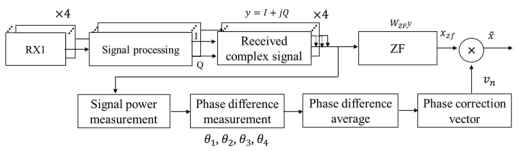


Fig.9. Improved ZF by symbol-by-symbol phase estimation

Therefore, one of the four receivers with the maximum SNR for TX1 is selected. Similarly, for TX2, TX3, and TX4, the receiver with the largest SNR for each transmitter is chosen to estimate the carrier phase. Assuming that the receivers with the largest SNR for each transmitter are TX1-RX1, TX2-RX3, TX3-RX4, and TX4-TX2, we used those preambles and postambles to compensate for the phase delay of each transmitted signal after ZF.

Next, We obtained the phase difference between the preamble and postamble of TX1-RX1, TX2-RX3, TX3-RX4, and TX4-TX2. Fig.10(d) shows the phase difference between the preamble and postamble of TX1 received at RX1. The phase difference $\theta_1,\theta_2,\theta_3,\theta_4$ between the preamble and postamble for TX1-RX1 is calculated, and their average value is obtained

$$\varnothing_1=\frac{\theta_1+\theta_2+\theta_3+\theta_4}{4}. \tag{20}$$

In the same way, the average value $\varnothing_2,\varnothing_3,\varnothing_4$ of the phase difference between the preamble and postamble of TX2-RX3, TX3-RX4, and TX4-RX2 is obtained. After performing ZF estimation, the order of the phase information is reversed because the received signal is multiplied by the inverse of the propagation matrix. $i$=1, ($i$ is the data number in the experiment: $i$=1,2,3, . . . $n$.) has the most advanced phase in the received signal, and $i$=$n$ has the most delayed phase. However, in the estimated signal after ZF, $i$=1 is the most behind, and $i$=$n$ is the most ahead. Therefore, the phase correction vector is generated using the average value of the phase difference $\varnothing_1, \varnothing_2, \varnothing_3, \varnothing_4$ of each transmitter as follows.

$$v_{1i}=\exp\left\{j\left(\frac{\varnothing_1}{2}-\frac{\varnothing_1 i}{n}\right)\right\} \tag{21a}$$

$$v_{2i}=\exp\left\{j\left(\frac{\varnothing_2}{2}-\frac{\varnothing_2 i}{n}\right)\right\} \tag{21b}$$

$$v_{3i}=\exp\left\{j\left(\frac{\varnothing_3}{2}-\frac{\varnothing_3 i}{n}\right)\right\}, \tag{21c}$$

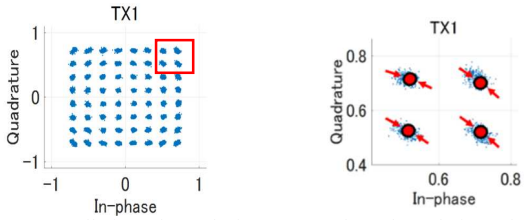


(a) Constellation of TX1 before phase correction vector multiplication. (b) Enlarged view of Fig.10(a).

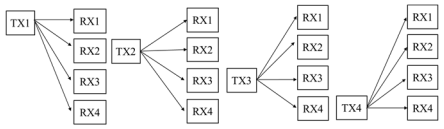


(c) Signal power detection diagram.

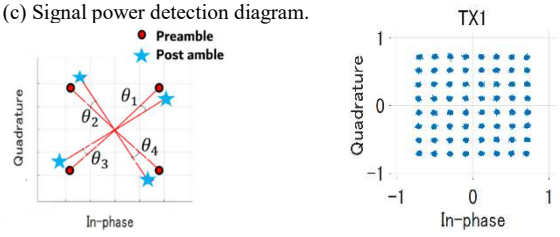


(d) Phase difference between preamble and postamble, for TX1. (e)Constellation of TX1 after multiplying by the phase correction vector

Fig.10. Improved ZF by symbol-by-symbol phase estimation.

$$v_{4i}=\exp\left\{j\left(\frac{\varnothing_4}{2}-\frac{\varnothing_{4i}}{n}\right)\right\}. \quad (21d)$$

As you can see from (21a) to (21d), the signal's phase after ZF at $i$=1 is delayed, so a vector is generated to advance the phase. Conversely, when $i$=$n$, the phase is most advanced, so the vector is generated to delay the phase. Then, the estimated signal after ZF ($x_{ZFsi}$) is multiplied by the phase correction vector for each transmitter.

$$x_{ZFsi}=[x_{1i}\ x_{2i}\ x_{3i}\ x_{4i}]^T \ (i=1.2.3...n.) \quad (22a)$$

$$\tilde{x}_{1i}=x_{1i}v_{1i} \quad (22b)$$

$$\tilde{x}_{2i}=x_{2i}v_{2i} \quad (22c)$$

$$\tilde{x}_{3i}=x_{3i}v_{3i} \quad (22d)$$

$$\tilde{x}_{4i}=x_{4i}v_{4i}. \quad (22e)$$

Fig.10(e) shows that the phase delay is corrected by multiplying the phase correction vector by TX1 after ZF. When using the DCO-OFDM system, phase correction vectors are generated for each subcarrier.

## III. Simulation and Experimental Results

### A. Simulation parameters

First, a computer simulation was performed to estimate the performance of the following experiments. The simulations calculated the rank of the propagation matrix and the SNR using the ZF method when the receiver moved in the $x$-$y$ plane. Table 1 shows the parameters of the single-carrier MIMO experiment, and Table 2 shows the parameters of the DCO-OFDM MIMO experiment. Fig.11(a) shows the top view of the optical receiver where $\theta_z$ is the rotation angle in the $x$-$y$ plane. Fig.11(b) shows the side view of the optical receiver where $\theta_r$ is the angle of tilt from directly above the receiver.

### B. Simulation results

Fig.12 shows the simulation results for the rank of the propagation matrix in the case of $\theta_z$ = 0 [deg], $\theta_z$ = 15, 30, 45 [deg]. $\theta_r$ was fixed at 30 degrees. In the simulation, the effect of noise is neglected. As shown in Fig.12(a), there is a point where the rank drops for $\theta_z$=0 [deg]. As shown in Figure 12(b), the case where $\theta_z$ was 15, 30, 45 degrees, was full rank.

TABLE 1 Parameters of Single-Carrier MIMO Experiment

| | |
|---|---|
| room size | 0.23×0.23(m) |
| MIMO system | 4×4 MIMO |
| LED wavelength | 630 nm |
| Modulation method | 64QAM |
| Symbol rate | 3.3 Msps |
| Transmission speed | 76 Mbps |

TABLE 2 Parameters of DCO-OFDM MIMO Experiment

| | |
|---|---|
| room size | 0.23×0.23(m) |
| MIMO system | 4×4 MIMO |
| LED wavelength | 630 nm |
| Modulation method | 64QAM |
| Symbol rate | 0.47 Msps |
| Transmission speed | 82 Mbps |
| Subcarrier spacing | 500kHz |
| Subcarrier number | 18 |
| GI ratio | 5.0% |

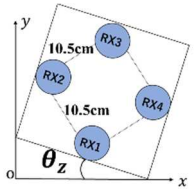


(a) Optical receiver (top view)

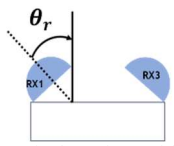


(b) Optical receiver (side view)

Fig.11. System model in the experiment.

Fig.13 shows the relationship between the SNR and $\theta_r$. The optical receiver moved by 1 cm step in the range of $x$=1~23(cm), $y$=1~23(cm) on the $x$-$y$ plane. Then the maximum and minimum SNR were plotted when $\theta_r$ was changed from 0 to 80 degrees. $\theta_z$ was fixed at 45 degrees. The difference between the maximum SNR and minimum SNR is smallest when $\theta_r$ = 65 [deg]. However, we conducted the experiments with $\theta_r$ = 30 [deg].

Fig.14 shows the maximum and minimum SNR using ZF measured when we changed the receiver position in the $x$-$y$ plane. In the simulations, we varied $\theta_z$ from 0 to 90 degrees. $\theta_r$ was fixed at 30 degrees. We see that the SNR deteriorates for $\theta_z$ = 0 [deg] due to the high correlation of the propagation matrix. In contrast, for $\theta_z$=45 [deg], the correlation of the propagation matrix is lower, resulting in a better SNR. From the simulation results shown in Fig.14, we experimented with the minimum SNR of the optical receiver angle $\theta_z$=0 [deg] and the maximum SNR of the angle $\theta_z$=45 [deg]. Fig.15 shows the theoretical relationship between the bit-error rate and the error vector magnitude (EVM) when 64QAM modulation is used.

### C. Single-Carrier 4×4 MIMO Experimental Results

We conducted the experiments under the following two conditions.

- Experiment 1 ($\theta_z$=0 [deg], $\theta_r$=30 [deg]): the distance from the optical transmitter to the receiver was fixed at 30 cm, and the optical receiver was placed at nine locations shown in Fig.16.

- Experiment 2 ($\theta_z$=45[deg], $\theta_r$=30[deg]): the distance from the optical transmitter to the receiver was fixed at 30 cm, and the optical receiver was placed at nine locations shown in Fig.16.

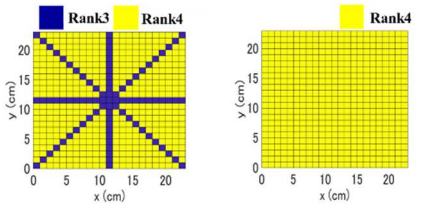


(a) $\theta_z$=0 [deg]. (b) $\theta_z$=15,30,45 [deg].

Fig.12. Relationship between optical receiver position and rank.

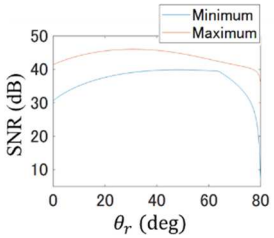


Fig.13. SNR vs. $\theta_r$ ($\theta_z$=45 [deg]).

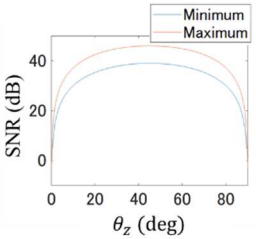


Fig. 14. SNR vs. $\theta_z$ ( $\theta_r$=30 [deg]).

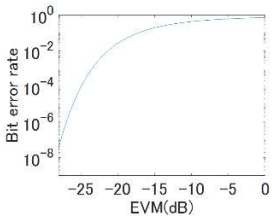


Fig.15. Bit error rate vs. EVM using 64QAM modulation.

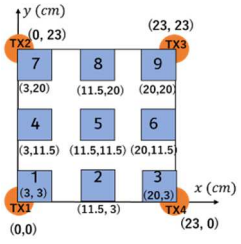


Fig.16. Location of a receiver and transmitter positions in the experiment.

Fig.17 shows a constellation diagram of the recovered signal in the single-carrier MIMO experiment with (a) ZF with the preamble, (b) ZF with the preamble and postamble, and (c) improved ZF by symbol-by-symbol phase estimation methods. Figs.18 and 19 show the relationship between the EVM and the position of the optical receiver in Experiment 1 and Experiment 2, respectively. In Figs.18 and 19, the numbers on the horizontal axis are the optical receiver positions corresponding to the numbers in Fig.16. From Fig.17, we see that the symbol-by-symbol phase estimation method is the most effective for recovering the original data.

In Experiment 1 ($\theta_z$=0 [deg].), the SNR degrades as in the simulation results, resulting in a degradation in the EVM value. The EVM results are almost the same in the ZF method with the preamble and postamble and improved ZF by symbol-by-symbol phase estimation. Still, transmission performance is degraded in the ZF method with the preamble compared to the other two cases. The results above indicate that phase correction with only a preamble is insufficient for data recovery.

In Experiment 2 ($\theta_z$=45 [deg].), improved ZF by symbol-by-symbol phase estimation shows an improvement in EVM compared to ZF with the preamble and ZF with the preamble and postamble. The results are because by improved ZF method by symbol-by-symbol phase estimation, we can appropriately compensate for the phase delay caused by the data order.

### *D. DCO-OFDM 4×4 MIMO Experimental Results*

- Experiment 1 ($\theta_z$=0 [deg], $\theta_r$=30 [deg]): the distance from the optical transmitter to the receiver was fixed at 25 cm, and the optical receiver was positioned at the nine locations shown in Fig.16.

- Experiment 2 ($\theta_z$=45 [deg], $\theta_r$=30 [deg]): the distance from the optical transmitter to the receiver was fixed at 25 cm, and the optical receiver was positioned at the nine locations shown in Fig.16.

Fig.20 shows a constellation diagram of each estimated signal in the DCO-OFDM MIMO experiment with (a)ZF with the preamble, (b) ZF with the preamble and postamble, and (c) improved ZF by symbol-by-symbol phase estimation, and Fig.21 and Fig.22 show the relationship between the EVM and the position of the optical receiver in Experiment 1 and Experiment 2, respectively. In (a), a recovered signal is slightly skewed, but the effect of the phase delay is less than for the single-carrier MIMO case. Due to the shorter data length in the case of OFDM, we could not identify the difference in the constellations in (b) and (c). In addition, constellation diagrams in Figs. 20 (a), (b), and (c) show that the OFDM signal is affected by nonlinearities due to the input-output characteristics of the LEDs.

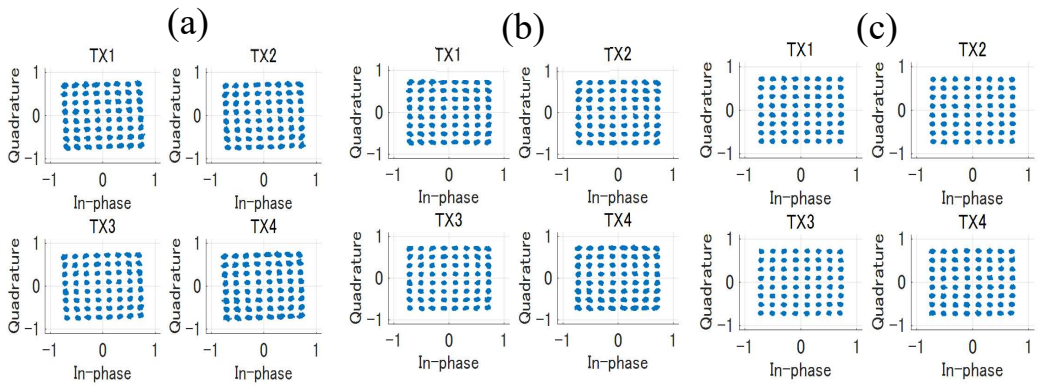


Fig.17.Constellation diagram of estimated signal in a single-carrier MIMO experiment. (a) ZF with the preamble, (b) ZF with the preamble and postamble, (c) improved ZF by symbol-by-symbol phase estimation.

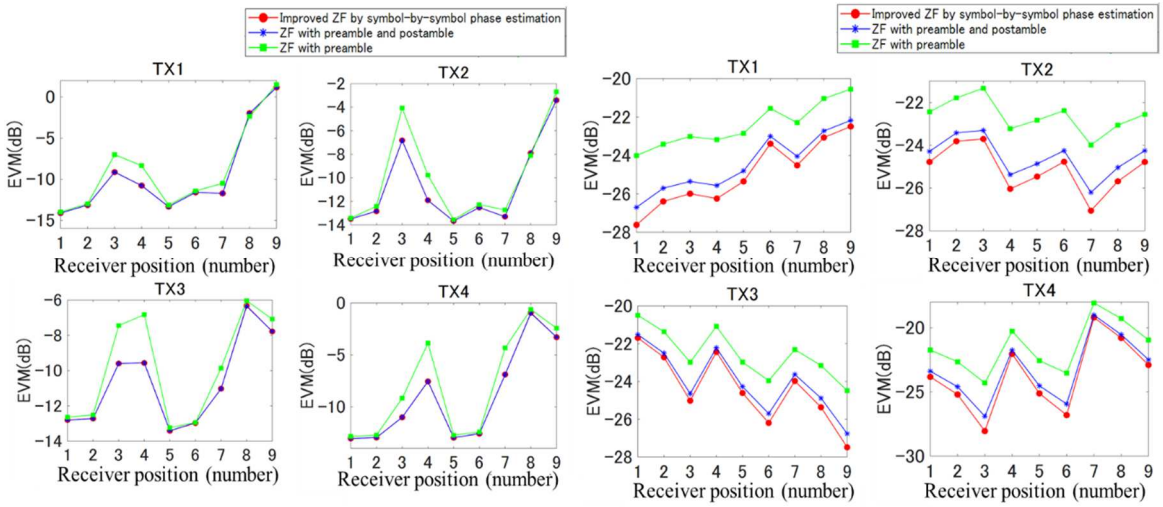


Fig.18. Relationship between EVM and optical receiver position in Experiment 1 ($\theta_z$=0 [deg]).

Fig.19. Relationship between EVM and optical receiver position in Experiment 2 ($\theta_z$=45 [deg]).

In the case of Experiment 1 ($\theta_z$=0 [deg].), the EVM results are almost the same for ZF with the preamble, ZF with the preamble and postamble, and improved ZF by symbol-by-symbol phase estimation. However, the ZF with the preamble slightly degrades compared to those two.

In Experiment 2 ($\theta_z$=45 [deg].), the EVM is almost the same for the improved ZF by symbol-by-symbol phase estimation and the ZF with a preamble and postamble. The OFDM signal has a shorter symbol length than the single-carrier signal, so the OFDM signal is less affected by the delay. In addition, it is not possible to obtain accurate preamble and postamble phase differences due to nonlinear effects when using OFDM. Therefore, EVM was not improved by using improved ZF by symbol-by-symbol phase estimation.

## Ⅳ. Conclusion.

We have compared three carrier phase estimation methods and confirmed that the symbol-by-symbol phase estimation method performs best. We believe that the phase correction method in this study will be more effective in the case of higher multi-level modulation formats such as 256QAM and 1024QAM.

## References


[1] T. Komine and M. Nakagawa, "Fundamental analysis for visible-light communication system using LED lights," IEEE Transactions on Consumer Electronics, Vol. 50, pp. 100-107, 2004.

[2] J. Grubor, S. Randel, K. -. Langer, and J. W. Walewski, "Bandwidth-efficient indoor optical wireless communications with white light-emitting diodes," 2008 6th International Symposium on Communication Systems, Networks and Digital Signal Processing, pp. 165-169, 2008.

[3] M. Aitao , Y. Guo, Y. Wang, and Z. Cao, "Indoor optical wireless MIMO System with non-imaging receivers," 2015 14th International Conference on Optical Communication Networks (ICOCN), Nanjing, China, pp. 1-4, 2015.

[4] Assaidah, O. C. Satya, H. Satria, Y. Adnan, K. Saleh and C. -W. Chow, "Analysis of DCO-OFDM application in MIMO-NOMA-VLC system serving 8 users," 2022 International Conference on Electrical Engineering, Computer and Information Technology (ICEECIT), Jember, Indonesia, pp. 01-04, 2022.

[5] Z Zhan *et al*., "1.2 Gbps non-imaging MIMO-OFDM scheme based VLC over indoor lighting LED arrangments," 2015 Opto-Electronics and Communications Conference (OECC), Shanghai, China, pp. 1-3, 2015.

[6] K. Rajeswari, T. Sangeetha, A. P. Natchammai, M. Nandhini and S. J. Thiruvengadam, "Performance analysis of pilot aided channel estimation methods for LTE system in time-selective channels," 2010 5th International Conference on Industrial and Information Systems, Mangalore, India, pp. 113-118, 2010.

[7] Z. Lu, P. Liu and S. Liu, "Experiment of beneficial clipping DCO-OFDM based visible light communication," 2017 IEEE 9th International Conference on Communication Software and Networks (ICCSN), Guangzhou, China, pp. 615-618, 2017.

[8] C. He, T. Q. Wang, and J. Armstrong, "MIMO optical wireless receiver using photodetectors with different fields of view," 2015 IEEE 81st Conference on Vehicle Technology, pp, 1-5, 2015.


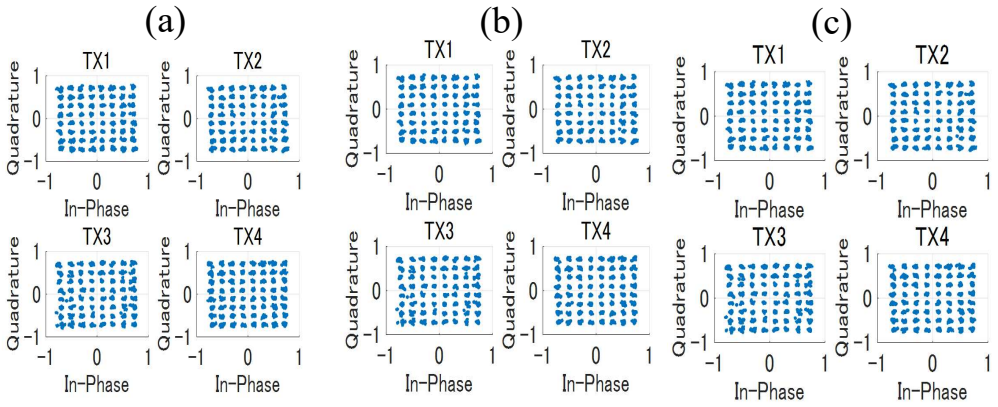


Fig.20.Constellation of each estimated signal in a DCO-OFDM MIMO experiment. (a) ZF with the preamble, (b) ZF with the preamble and postamble, (c) improved ZF by symbol-by-symbol phase estimation.

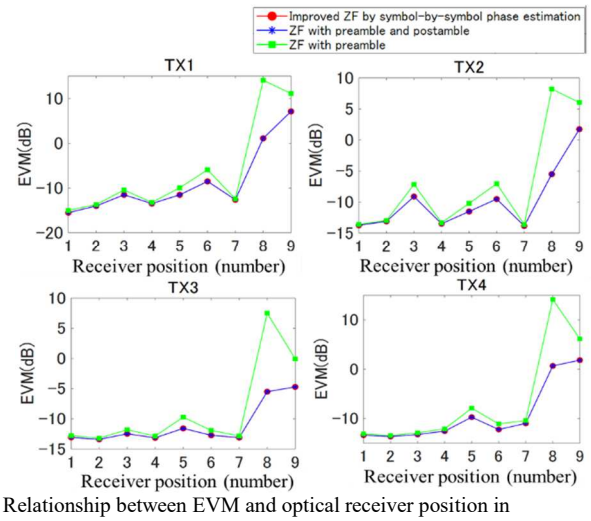


Fig.21. Relationship between EVM and optical receiver position in Experiment 1 ($\theta_z$=0 [deg]).

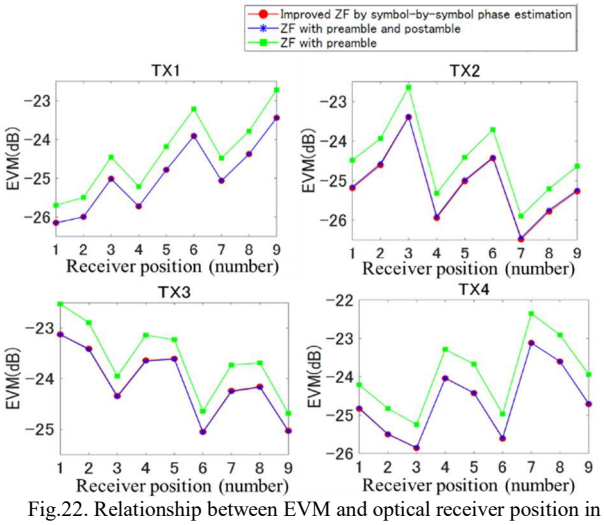


Fig.22. Relationship between EVM and optical receiver position in Experiment 2 ($\theta_z$=45 [deg]).